Journal of Colloid and Interface Science 684 (2025) 225–234

Contents lists available at ScienceDirect

Journal of Colloid And Interface Science

journal homepage: www.elsevier.com/locate/jcis

Understanding drug solubilization in intestinal mixed micelles through molecular dynamics simulations

Fatmegyul Mustan [a,*], Nikola Genchev [a], Liliya Vinarova [a], Jan Bevernage [c], Christophe Tistaert [c], Anela Ivanova [b], Slavka Tcholakova [a], Zahari Vinarov [a]

[a] Department of Chemical and Pharmaceutical Engineering, Faculty of Chemistry and Pharmacy, University of Sofia, Bulgaria
[b] Department of Physical Chemistry, Faculty of Chemistry and Pharmacy, University of Sofia, Bulgaria
[c] Janssen Pharmaceutica NV, Beerse, Belgium

GRAPHICAL ABSTRACT

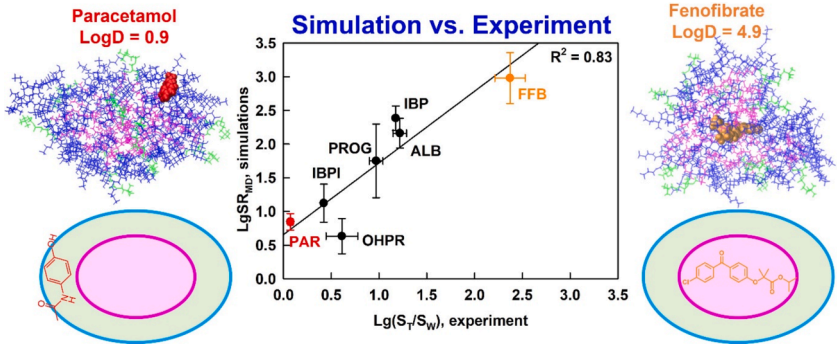

ARTICLE INFO

Keywords:
Solubilization
Drug lipophilicity
Molecular dynamics
Orientation
Palisade layer
Hydrophobic core
Experimental verification

ABSTRACT

Hypothesis: Solubilization is a fundamental process that underpins various technologies in the pharmaceutical and chemical industry. However, knowledge of the location, orientation and interactions of solubilized molecules in the micelles is still limited. We expect all-atom molecular dynamics simulations to improve the molecular-level understanding of solubilization and to enable its *in silico* prediction.

Methods: The solubilization of six drugs in intestinal mixed micelles composed of taurocholate and dioleoyl phosphatidylcholine was simulated by molecular dynamics in explicit water and measured experimentally by liquid chromatography. The location and orientation of the solubilized drugs were visualized by cumulative radial distribution functions and interactions were characterized by radial distribution function ratios and hydrogen bonding.

Findings: A new simulation-derived parameter was defined, which accounts for drug-micelle and drug-water interactions and correlates (R^2 = 0.83) with the experimentally measured solubilization. Lipophilicity was found to govern the location of all drugs in the micelle (hydrophobic core, palisade layer or on the surface), while hydrogen bonding was crucial for orientation and solubilization of two of the molecules. The study demonstrates that explicit, hydrogen bond-forming water molecules are vital for accurate prediction of solubilization and

* Corresponding author at: Department of Chemical and Pharmaceutical Engineering, Faculty of Chemistry and Pharmacy, Sofia University "St. Kl. Ohridski", 1 James Bourchier blvd., 1164 Sofia, Bulgaria.
E-mail address: fm@lcpe.uni-sofia.bg (F. Mustan).

https://doi.org/10.1016/j.jcis.2025.01.088
Received 12 September 2024; Received in revised form 9 January 2025; Accepted 11 January 2025
Available online 13 January 2025

provides a comprehensive framework for quantitative studies of drug location and orientation within the micelles.

1. Introduction

The overall absorption of drugs *in vivo* after oral administration depends on the balance between two main factors [1]: the drug solubility in water and its membrane permeability. Drug solubilization is known to impact both of these factors [1–3] and is one of the key parameters that should be measured (or predicted) when the various absorption-related processes are considered during drug development [4–6].

In the small intestine, where the majority of drug absorption occurs, poorly water-soluble drugs are solubilized by endogenous mixed micelles composed of bile salts, phospholipids and other minor components [7]. Solubilization can increase intestinal drug concentrations by several orders of magnitude, especially for practically insoluble molecules that are frequently generated from the drug discovery pipelines [8–11]. This solubility-enhancing effect is an integral part in the *in silico* prediction of oral drug pharmacokinetics [12–14].

However, the molecular-level understanding of the process, which should include a clear link between drug structure and the experimentally measured solubilization in biorelevant micelles, is still missing. Very limited data about the locus of drug solubilization in the bile micelles (hydrophobic core, palisade layer or micelle surface) is available and even less studies have assessed the orientation of the solubilized drugs [15,16].

Molecular dynamics (MD) simulations are one of the main techniques which can provide information at such level [17], including the relative location and orientation of the molecules in the micelles. This tool has been applied to study drug solubilization in bile salt phospholipid micelles and was recently reviewed with respect to its application in the study of lipid-based drug formulations [18] and drug solubilization in pharmaceutical systems [19].

More than a decade ago, the spontaneous aggregation of sodium cholate (CH) and palmitoyl oleoyl phosphatidylcholine (POPC) at ratios of 2:1 and 1:1 was monitored by MD simulations with a united atom model for the hydrogens bound to carbon atoms [20]. The authors obtained slightly ellipsoidal aggregates with radii r_{max} = 2.4–2.5 nm and r_{min} = 2.0–2.1 nm, and described the structure of the micelle by a radial shell model, where the tails of the phospholipid are oriented radially toward the center of the micelles, while the bile molecules sit at the surface and fill the space between the phospholipid headgroups. Identical assembly of cholic acid and dodecyl phosphocholine molecules was shown by fully atomistic MD simulations [21]. Prolate mixed micelles were formed, stabilized by hydrogen bonding between the two types of molecules. Micelle sizes in the same range were obtained by coarse-grain simulations of different versions of the simulated intestinal fluids [22,23]. Additionally, the solubilization of cholesterol in such a mixed micelle was simulated and no significant change in the shape and size of the micelles was found. It was shown by radial distribution functions that cholesterol is situated into the hydrophobic core of the micelles [20]. Solubilization of danazol inside the hydrophobic core of mixed micelles of sodium glycodeoxycholate and digested triglyceride was also simulated by united-atom MD simulations. Good qualitative agreement between experiments and MD simulations was shown. The solubilization of danazol increases with the increase of lipid digestion products in the simulated mixed micelles [24].

Coarse-grained MD simulations were used to calculate the affinity of prednisolone, fenofibrate and probucol into intestinal ellipsoidal micelles containing bile salts, phospholipids, free fatty acids, and cholesterol with size ranging from 2 to 7 nm. The results were in qualitative agreement with experimental solubility data from the literature [16,25].

However, the interactions of the aforementioned solubilized substances with the surrounding molecules were not discussed in more detail except for the contacts between them, but they are crucial for revealing the driving forces of the process.

As such, mechanistic data about the solubilization of different drugs is scattered and is usually obtained by using different methodology (e.g. atomistic vs. coarse-grained simulations), which complicates comparison and confounds interpretation. There are no studies so far about the role on solubilization of small functional groups attached to the same molecular base structure.

In this study, we investigate systematically the driving force for drug solubilization by estimating the drug location and orientation in the micelles and its interactions with the aqueous media. The validity of the simulation results is backed up by verification against experimental data. The solubilization of six poorly water-soluble drug molecules (including two identical molecules differing by only one OH group) in a biorelevant mixed micelle composed of taurocholate (TC) and dioleoyl phosphatidylcholine (DOPC) is studied by all-atom MD simulations and the results are compared to the degree of solubilization as measured by ultra-high performance liquid chromatography (UPLC). The conclusions drawn may be applied in a more general context because dependence of the solubilization on fundamental physical chemical characteristics is outlined.

2. Materials and methods

2.1. Materials

The following six poorly water-soluble drug molecules were studied: albendazole (ALB), fenofibrate (FFB), ibuprofen (IBP), 17-OH-progesterone (OHPR), paracetamol (PAR), and progesterone (PROG). Their main characteristics and chemical structures are presented in Table 1. All used substances are with purity above 98 %, except for OHPR with purity > 95 %.

Biorelevant media was prepared by using 3F powder (Biorelevant.com Ltd, UK), which is a freeze-dried 4:1 (molar ratio) mixture of sodium taurocholate and soy lecithin, dissolved in acetate buffer. The latter contains NaCl (99 %, product of Sigma), glacial CH_3COOH (product of Merck) and NaOH (product of Honeywell).

Methanol (RPE, product of Carlo Erba) was used for sample dilution and standard preparation prior to UPLC analysis.

Mobile phase solvents include acetonitrile (HPLC PLUS Gradient grade, product of Carlo Erba) and trifluoroacetic acid (>99 %, product of TCI) solution in water. All aqueous solutions and phases were prepared with deionized water from an Elix 3 water purification system (Millipore, USA).

2.2. Experimental measurements

Drug solubilization was measured in fed-state biorelevant media. To calculate the solubilization ratio, aqueous drug solubility data was also required. Hence, it was determined in the blank buffer, which was used to dissolve the biorelevant components. Briefly, excess of drug was weighed in a 10 mL glass bottle and 6 mL of acetate buffer (pH = 5.0) or fed state simulated intestinal fluids (FeSSIF) biorelevant medium were added. FeSSIF medium was prepared by dissolving an appropriate amount of 3F powder to obtain 15 mM taurocholate and 3.75 mM phospholipid solution at pH = 5.0. To keep constant pH = 5.0 during the experiment, acetate buffer containing 203.1 mM NaCl, 144 mM glacial CH_3COOH and 101 mM NaOH was used. The obtained suspensions were homogenized for 24 h at 37 °C by shaking at 400 rpm using a Thermomixer C (Eppendorf SE, USA). Afterwards, the undissolved solids were removed by centrifugation for 5 min at 20,000*g* at 37 °C and

aqueous drug concentrations were determined by UPLC after ten-fold dilution in methanol. All experiments were performed at least in duplicate.

UPLC analysis was carried out on a Nexera Shimadzu apparatus, equipped with solvent delivery module (LC-40D x3), autosampler (SIL-40C x3) and a photodiode array (PDA) detector (SPD-M40). An Acquity UPLC® BEH C18 column with pore size of 130 Å, particle size of 1.7 μm, inner diameter of 2.1 mm and 50 mm length was used for analysis with Acquity UPLC® BEH C18 VanGard pre-column (2.1 mm × 5 mm, 1.7 μm) at 50 °C. For the analysis of most of the studied drugs (ALB, FFB, IBP, OHPR, PROG), a binary gradient of 0.1 % trifluoroacetic acid (TFA) and acetonitrile (ACN) at a 1 mL/min flow rate was used (Table S1 in the Supporting information (SI)). Injection volume was set to 1 μL.

For the analysis of paracetamol, Waters X-bridge C18 analytical column (150 mm × 4.6 mm, 3.5 μm), connected to a Waters VanGard C18 guard column (3.9 mm × 5 mm, 3.5 μm) was used. The mobile phase was ACN – 0.1 % TFA at a volume ratio of 10:90. Isocratic elution with flow rate of 1 mL/min and injection volume of 0.1 μL was used.

The concentration of solubilized drug was determined by using a standard curve ($R^2 = 0.999$), which was prepared by dissolving a known amount of drug in methanol–water mixture (9:1).

2.3. Molecular models and computational protocol

A. Molecular models

Model systems containing one mixed micelle built of 40 molecules of sodium TC and 10 molecules of DOPC were simulated in explicit water in the presence of a single drug molecule. The molecules of TC, FFB, ALB, IBP, PAR, PROG, as well as Na^+ and Cl^- ions, are described with the force field AMBER99 [26], the molecules of DOPC and OHPR are described with the force field Lipid 17 [27]. The model TIP4P [28] is used for water. DOPC is one of the default molecules in Lipid 17, that is why its topology and parameters were directly taken from the force field library. The force field parameters for TC were reported previously [29]. The parameters for all drug molecules were taken from the force fields AMBER99 [26] and Lipid17 [27], and missing parameters were adopted from the GAFF force field [30]. The parameter files and optimized structures of the drug molecules are accessible in the *Zenodo* platform https://doi.org/10.5281/zenodo.14605820.

For this purpose, conformational search and geometry optimization of the representative structures with the DFT functional B3LYP [31,32] and basis set 6-31G* [33] was performed. The RESP (Restrained ElectroStatic Potential) [34,35] procedure was applied to calculate the atomic partial charges, where the charges were fitted to the quantum mechanical electrostatic potential of each molecule, generated at the HF/6-31G* level. The final RESP charges were averaged over the most stable conformers of each molecule.

To construct the model systems, an MD simulation of an aqueous solution of TC (40 molecules) and DOPC (10 molecules) randomly placed as monomers was performed to obtain a spontaneously formed mixed micelle at the desired experimental ratio of 4:1 between TC and DOPC. This simulation was performed in a cubic periodic box with an edge size of 6 nm. Three independent simulations of the formation of the micelle were run to calculate average micelle properties.

To assess the equilibration of the single micelle obtained in each of the three trajectories, the root-mean-square deviation of the coordinates from the initial position was analyzed, which fluctuated about a constant value after 50 ns of the simulations. Additionally, the number of the molecules included in the micelle was monitored with time. A constant number of 50 molecules after 50 ns of the simulation was attained, indicating stable composition of the formed mixed micelle. The results from the three independent simulations of the empty micelle were identical, showing no preference for which of the micelles would be chosen for the next stage of the study. Therefore, the final snapshot at 300 ns of the mixed TC:DOPC micelle from the first simulation was used to construct the models in the presence of a drug molecule. The micelle was placed at the center of a cubic box with an edge size of 8 nm. The drug molecule was located near the micelle in the simulation box at three or four (in case of OHPR and ALB) different initial positions (Fig. S1 in the SI). Then, water molecules and Na^+ and Cl^- ions at concentration of 145 mM were added to match the experimental conditions,

Table 1
Main properties of the studied drug molecules.

Drug	Abbreviation in the text	Molecular structure	Molar mass, g/mol	Solubility in water, mg/ml	Log*P*	Supplier
Albendazole	ALB	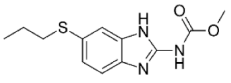	265.3	0.002	3.2	TCI
Fenofibrate	FFB	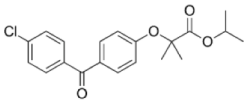	360.8	0.001	4.9	Sigma
Ibuprofen	IBP	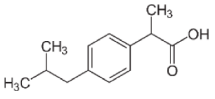	206.3	0.021	3.8	Donated by Actavis
17-OH progesterone	OHPR	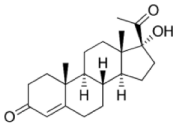	330.5	0.029	3.0	Sigma
Paracetamol	PAR	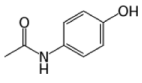	151.2	14.000	0.9	Sigma
Progesterone	PROG	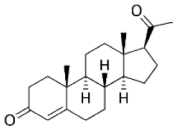	314.5	0.005	3.6	TCI

which corresponds to 45 'molecules' of NaCl calculated by the following relation $N = CN_AV$, where N is the number of ions added in the simulation box, C is the concentration (145 mM), N_A is Avogadro's number ($6.02x10^{23}$ mol^{-1}), and V is the volume of the simulation box (512 nm^3). Note, upon construction of the systems we used the default GROMACS command (*gmx genion*) to calculate the number of the desired ions by providing the relevant concentration. Additional sodium ions were added to neutralize the charge of taurocholate anions, corresponding to the experimental studies, in which the sodium salt of taurocholate is used.

B. Computational protocol

The following computational protocol was employed for all systems: (*i*) energy minimization with the algorithm L-BFGS [36]; (*ii*) heating to 310 K in NVT ensemble with Berendsen thermostat with coupling time of 0.1 ps [37]; (*iii*) relaxation for 1 ns in NVT ensemble at 310 K; (*iv*) production runs for 300 ns with time step 2 fs in NVT ensemble. Snapshots were saved in the trajectories at intervals of 5 ps. NVT ensemble was used in order to keep constant concentrations of the components in the solution. Comparative simulations (NVT vs. NPT ensemble) showed no significant difference in the results for FFB solubilization. The influence of the chosen thermostat was also checked, by comparing the Berendsen thermostat to the V-rescale variant for one of the studied systems (solubilization of FFB). The results showed no significant difference in the calculated solubilization parameter, $LgSR_{MD}$ (see the following subsection for its definition). The algorithm leapfrog [38] was used to integrate the equations of motion during heating, relaxation and production runs. The lengths of all hydrogen-containing bonds were fixed with LINCS [39] (for the TC, phospholipid, and drugs) and SETTLE (for the water molecules) [40]. The non-bonded interactions were described by a Lennard-Jones potential and a Coulomb term at cutoff 12 Å with a switch function initiated at 10 Å. Long-range electrostatic interactions were evaluated with the PME method [41,42]. The GROMACS 2021.3 program package [43] was used for all simulations and analysis, whereas VMD was employed for visualization of the trajectories [44].

C. Analysis of the MD trajectories and data processing

Equilibration of the systems was verified by monitoring the evolution of system energy and root-mean-square deviation of the coordinates of the micelle and the number of contacts between the micelle and the drug molecule. All these parameters started to fluctuate around a constant value after ≈ 100 ns. Therefore, analysis for determination of the solubilization and for characterization of the interactions between drug and micelles were conducted in the last 100 ns (from 200 to 300 ns) of the trajectories, in which no dramatic changes in the molecular configurations occur, thus avoiding fluctuations in the analyses.

Hydrogen bonds were analyzed by using the default GROMACS program *gmx hbond* with the geometrical criterion about the distance and angle between the hydrogen donor and acceptor: $r \leq r_{HB} = 0.35$ nm for donor–acceptor distance and the angle donor – hydrogen – acceptor should not deviate more than 30° from the ideal angle which is 180°.

The most probable location of the drug molecules in the micelle (hydrophobic core, palisade layer or micelle surface) was determined by studying the cumulative distribution functions, whereas solubilization was calculated by considering the whole micelle via the radial distribution functions (RDF). In this way, we analyzed separately the location and solubilization of the drug molecule, reducing uncertainty in cases where the solubilized molecule can be found simultaneously in two regions of the micelle (e.g. when a part of the molecule is in the hydrophobic core, while another part reaches the palisade layer). The latter was a frequent phenomenon, because the radius of the studied micelle was of the same order of magnitude as the size of the solubilized molecule.

To calculate the solubilization of the drugs from the generated MD trajectories, RDF between the center of geometries (COG) of the drug and micelle ($RDF_{D\text{-}M}$), and COG of drug and water ($RDF_{D\text{-}W}$) were analyzed and processed to calculate the area of the first peak up to $r =$ 0.6 nm (Fig. S2A,B in the SI), which is a typical cut-off for short-range interactions, corresponding to the sum of the Van der Waals radii of two CH groups (0.58 nm) [45], which are responsible for hydrophobic interactions with the first neighbors. Expanding further the cutoff, e.g. to 1.5 nm, takes almost the whole RDF profile and includes long-range interactions, which diminishes the sensitivity of the method. Therefore, the 0.6 nm cut-off was used for the calculations below.

The obtained values for RDF areas (drug-micelle and drug-water) were then divided to calculate $LgSR_{MD}$ (Eq. (1)), which quantifies the affinity of the drug to the micelle [25]:

$$LgSR_{MD} = \lg\left(\frac{\sum_{r=0}^{0.6} RDF_{D-M}}{\sum_{r=0}^{0.6} RDF_{D-W}}\right) \quad (1)$$

$LgSR_{MD}$ was calculated for each separate simulation of each drug at three different initial positions in the simulation box and the obtained results were used to calculate the average and standard deviation.

The proposed approach can be used for spherical micelles with any size and composition. To be applied for worm-like or disk-like micelles instead of RDFs more general pair distribution functions should be calculated depending on the shape of micelles, e.g. cylindrical coordinates should be used for worm-like micelles.

3. Results and Discussion

The experimental results about drug solubilization are presented first, followed by the results from the MD simulations in terms of micelle composition and morphology, solubilization of the drug molecules, and intermolecular interactions.

3.1. Experimental results

Solubilization in FeSSIF and aqueous solubility at pH = 5.0 of the studied drugs was determined via UPLC (Table 2). The obtained values were used to calculate the solubility enhancement (SE) using the ratio $SE = S_T/S_W$, where S_T is the experimentally measured solubility of the drug after solubilization in FeSSIF micelles and S_W is the aqueous drug solubility at pH = 5.0.

Considering a micelle aggregation number of 62 [46], the number of solubilized drug molecules per micelle can be calculated (Table 2). The results showed that for four of the six studied drugs, the solubilized number of drug molecules per micelle is less than one, which means that the used molecular model for the MD simulations (one drug molecule per micelle) is relevant and can be compared to the experiment. For IBP and PAR, which show significantly bigger number of drug molecules per micelle, drug-drug interactions cannot be captured by the used simulation protocol.

Table 2
Experimental data for drug solubilization and aqueous solubility. Ibuprofen was measured both at standard conditions (pH = 5.0), at which it is negatively charged, and in acidified media (pH = 3.0) to study the solubilization of the neutral form.

Drug	Solubility in FeSSIF, pH= 5.0 (S_T), μg/ml	Solubility at pH = 5.0 (S_W), μg/ml	Solubility enhancement, Lg (S_T/S_W)	Number of drug molecules per micelle (N_{agg} = 62)
ALB	11.4 ± 0.3	0.69 ± 0.11	1.22 ± 0.07	0.14 ± 0.004
FFB	44 ± 7	0.19 ± 0.06	2.37 ± 0.16	0.42 ± 0.07
IBP	1550 ± 35	587 ± 11	0.42 ± 0.01	16.3 ± 0.6
$IBP_{pH=3}$	957 ± 18	64 ± 2	1.17 ± 0.02	15.1 ± 0.3
OHPR	29 ± 11	7.1 ± 0.4	0.61 ± 0.17	0.23 ± 0.12
PAR	21850 ± 660	18500 ± 970	0.07 ± 0.03	77 ± 27
PROG	98 ± 8	10.5 ± 1.5	0.97 ± 0.07	0.97 ± 0.09

3.2. Molecular dynamics simulations

A. Morphology and composition of the micelles

To gain insight on how polarity varies within the micelle, a hydrophilic and hydrophobic part was defined for the TC and DOPC molecules. For the bile salt, the condensed steroid backbone (without the OH-groups) was marked as hydrophobic, whereas the taurine part was labelled as hydrophilic. For DOPC, the two oleic chains were used to denote the hydrophobic part whereas the phosphatidylcholine moiety was marked as hydrophilic (Fig. 1A).

Based on the approach described above, the cumulative RDF with respect to the geometrical center of the micelle was calculated for the hydrophilic and hydrophobic moieties of TC and DOPC, as well as for the water molecules. The obtained results were averaged for the three trajectories of the empty micelle (Fig. S3 in the SI) and for all systems studied with different drugs in the drug-loaded micelle (Fig. 1B).

This analysis allowed us to determine the boundaries and sizes of the hydrophobic core, the palisade layer, and the entire micelle (Table S2 in the SI). The position of the interface between the hydrophobic core and the palisade layer was defined as the distance from the micelle center, at which the concentration of water molecules equals 1 %. On the other hand, the outer surface of the micelle was defined at 90 % of the taurine residue, which was the outermost component. This analysis yields 3.13 ± 0.13 nm and 2.99 ± 0.09 nm for the size of the empty and drug-loaded micelles, respectively (Table S2 in the SI). Similar results were obtained by Clulow et al. [23] with DLS measurements of FeSSIF solutions (3.35 ± 0.7 nm). This agreement suggests that cumulative RDF may provide a valid estimation of micelle hydrodynamic radius. Detailed data for the size of the micelle is provided in the SI (Section "*Micelle size*").

In the empty micelle, the oleic acid chains of DOPC were spread across the hydrophobic core and the palisade layer, whereas the steroid skeleton of TC was at the boundary between these two parts of the micelle. The palisade layer included also the taurine moiety of TC (oriented towards the surface of the micelle) and the phosphatidylcholine part of DOPC. Similar arrangement of the molecules was determined for the mixed micelles of POPC and cholate: radially packed phospholipids with tails toward the center of the micelle, surrounded by bile salt molecules, which were exposed to the aqueous media with their hydrophilic face [20].

The size of the micelle was not affected significantly by the drug solubilization (Table S2 in the SI). However, the drug-loaded micelle was characterized by a clearer composition of the hydrophobic core, which contained close to 100 % of the DOPC oleic acid chains and ≈ 60 % of the hydrophobic part of TC. Accordingly, the palisade layer was composed mainly of the hydrophilic taurine part of TC and the polar phosphatidylcholine moiety of DOPC. This change in the molecular organization of the drug-loaded micelle (compared to the empty micelle) was in agreement with the more elongated shape of drug-loaded micelle (described in Section "*Micelle shape*" in the SI). Similar micelle shapes have also been measured experimentally [47,48].

B. Position of the drug in the micelle

The standard approach to assess and visualize the position of drug molecules in the micelle is to analyze the final frames of the MD simulations (t = 300 ns, Fig. S4 in the SI). However, in reality, the position of the solubilized drug molecule is not constant, as all molecules (drug, TC and DOPC) are very dynamic and the configuration varies with time, as illustrated by the evolution of the number of contacts between drug and micelle (Fig. S5 of the SI).

To account for the dynamics of the molecules, the position of the drug solubilized in the micelle was determined via cumulative number RDF. The analysis was performed for all replicates of each drug-micelle system and the obtained data over the last 100 ns (see *Analysis of the MD trajectories and data processing*) were averaged. In this way, a statistically-sound analysis and visualization of the most probable location and orientation of each drug molecule within the micelle was obtained (Fig. 2).

FFB was found to be solubilized into the hydrophobic core of the micelle, surrounded by the oleic acid chains of DOPC. This location was confirmed experimentally by UV–Vis spectrometry, which indicated non-polar, alkane-like microenvironment of FFB solubilized in FeSSIF micelles (Fig. S6 in SI).

The hydrophobic fragments of IBP ($C_2H_3(CH_3)_2$) were solubilized in the hydrophobic core, whereas its polar group (COOH) was located at the interface between the hydrophobic core and the palisade layer. The orientation of the molecule was perpendicular to the surface of the micelle: the hydrophobic part was in the hydrophobic core, entirely screened from the water, whereas the polar group containing oxygen atoms was oriented outwards, reaching the palisade layer where it had access to water. It is important to note that at experimental pH = 5 more than 50 % of IBP is ionized. Thus, a double check about the effect of ionization was done by (1) simulations with both neutral (IBP) and ionized (IBPI) form of ibuprofen and (2) solubilization experiments at pH = 3 where the ibuprofen molecules were protonated. We observed a

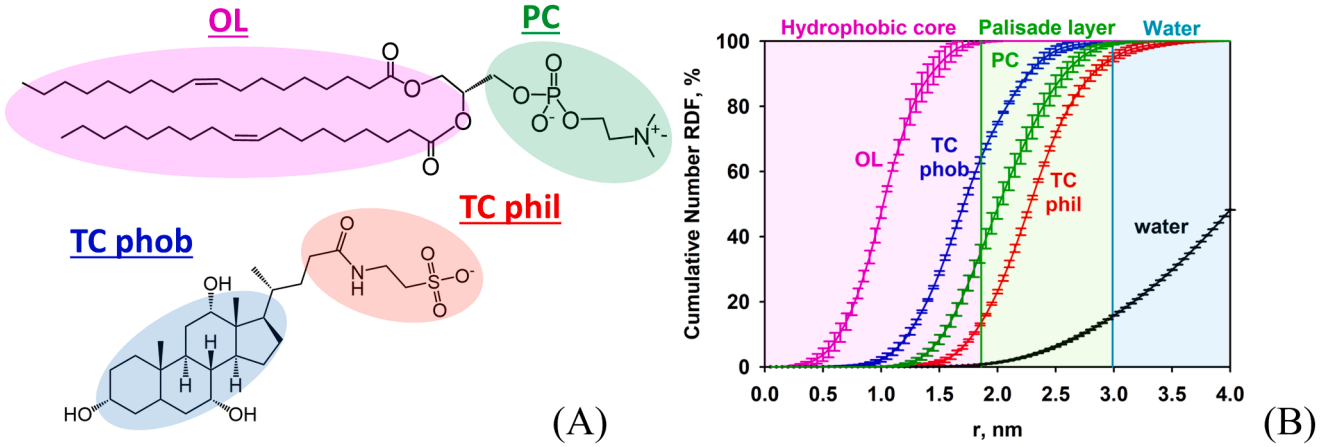

Fig. 1. (A) Chemical structures of DOPC (up) and TC (down) with colored hydrophilic and hydrophobic parts used in the analysis. (B) Cumulative number RDF between the geometrical center of the micelle and system components in the drug-loaded micelle averaged from 20 simulations. The functions are calculated for the last 100 ns of the simulation for the following fragments: taurine residue of TC (red lines), steroid skeleton of TC (blue lines), oleic tails of DOPC (pink lines), phosphatidylcholine head of DOPC (green lines), water (black lines). Colored areas on the plots represent: hydrophobic core of the micelle (pink), the palisade layer (green) and the aqueous media (blue). (For interpretation of the references to colour in this figure legend, the reader is referred to the web version of this article.)

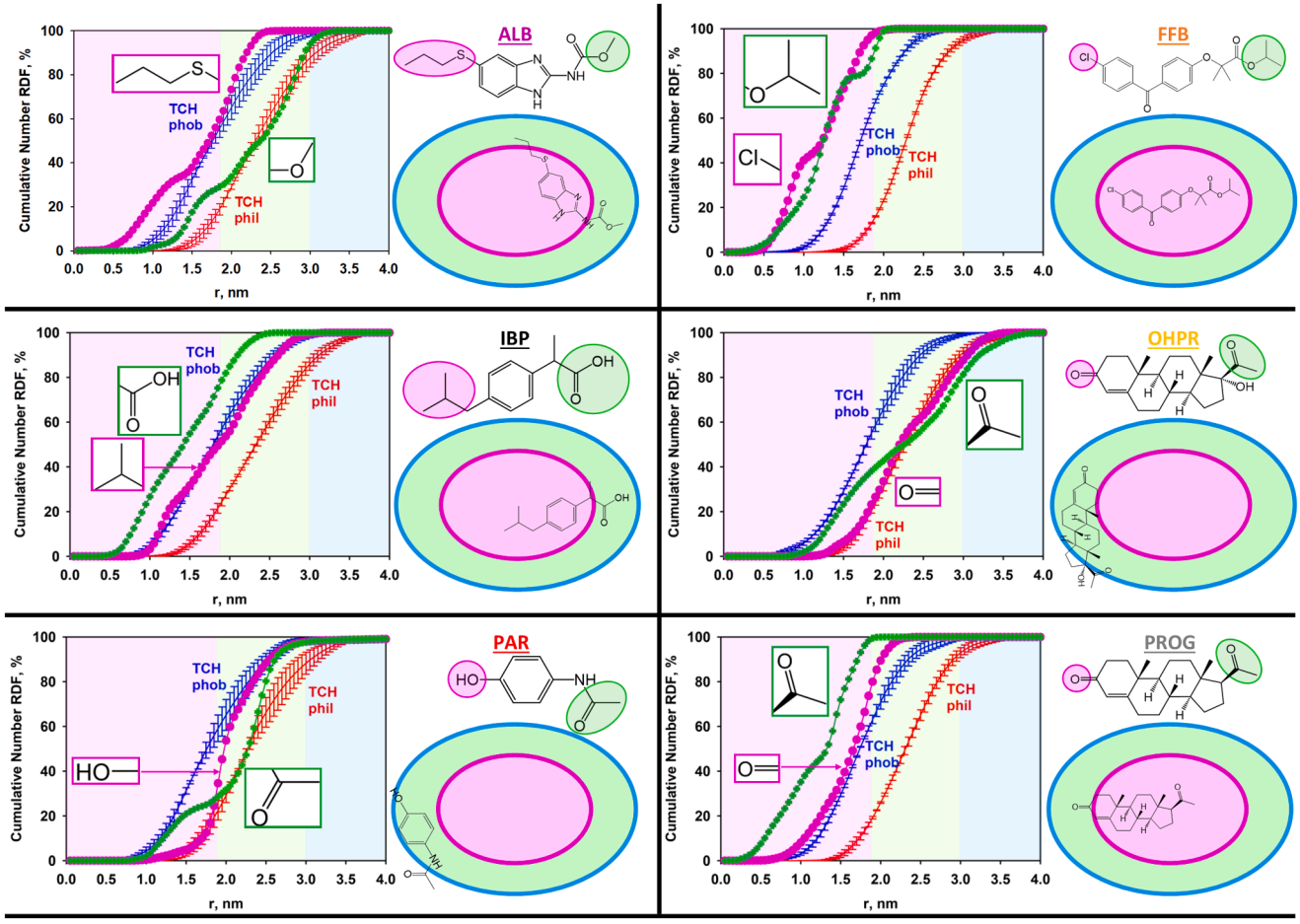

Fig. 2. Cumulative number RDF between the geometrical center of the micelle and system components: taurine residue of TC (red lines), steroid skeleton of TC (blue lines), and drug fragments (pink and green circles) shown on the chemical structures and schematic representation of the micelles with solubilized drugs. The pink area in the plots and illustrations denotes the hydrophobic core; the green area, the palisade layer; the blue area, the water medium. (For interpretation of the references to colour in this figure legend, the reader is referred to the web version of this article.)

change in the location in the micelle of the neutral and ionized forms of ibuprofen: the ionized form preferred being near the surface of the micelle, in contrast to the neutral form (Fig. S7 in the SI).

The orientation of PROG in the micelle was very similar to IBP. The hydrophobic $COCH_3$ part was solubilized in the hydrophobic core, whereas the CO group (attached to the steroid backbone) was located at the interface between the hydrophobic core and the palisade layer.

Interestingly, the orientation of OHPR (Fig. 2) was almost completely reversed, compared to PROG. The presence of one OH-group near the $COCH_3$ moiety switched its location from the hydrophobic core (for PROG) to the palisade layer, near the micelle surface (for OHPR). This finding demonstrates that a single hydroxyl group can have a dramatic impact on the location and orientation of solubilized molecules. In addition, the results presented in Table 2 showed that the addition of the hydroxyl group caused a three-fold decrease in solubilization. It can thus be concluded that hydroxyl group reduces solubilization and can alter the location of solubilized molecules, bringing them closer to the micelle surface where they can contact water molecules.

A very clear orientation was observed also for ALB. In that case, the nonpolar part of the molecule, containing sulfur atoms and a saturated propyl residue, was found between the core and palisade layer, and the polar part with an amide group was at the surface of the micelle.

Paracetamol, being the most hydrophilic molecule with the highest solubility in water among the 6 studied drugs, had no preferable orientation with respect to the micelle and was present in the palisade layer. This was probably related to the fact that this molecule is relatively small (compared to the rest) and both ends contain polar groups: amide and hydroxyl residues at *para*-position of the phenyl ring.

Drug location in the micelle was found to depend on drug lipophilicity, which is visualized as a correlation plot between the most probable distance of the drug from the center of the micelle and Log*P* (Fig. S8G in the SI). This distance was determined from the peak of the RDF denoting the location of the whole drug molecule relative to the geometrical center of the micelle (Fig. S8A-F in the SI).

C. Analysis of drug solubilization and experimental verification

Building upon the work of Parrow *et al.* [25], we used the ratio between the drug-micelle and drug-water contacts, obtained from the corresponding RDF in the MD simulations, to calculate $LgSR_{MD}$ (see Section 2.3.*C* and Eq. (1). $LgSR_{MD}$ was then correlated to SE: the experimentally determined solubilization, expressed as the ratio of the total measured apparent solubility and the aqueous drug solubility at the same pH and at constant surfactant concentration (see section 3.1). A good correlation between the MD-simulated and the experimentally determined solubility enhancement was obtained, Fig. 3.

It should be noted that both states of IBP (neutral and negatively charged) are part of the correlation (Fig. 3) but appear at different coordinates. This is due to the different solubilization of the neutral (pH = 3) and charged form (pH = 5), as determined experimentally and in the MD simulations. Hence, the used methodology appears to account also for the effects of electrostatic interactions between the charged micelle

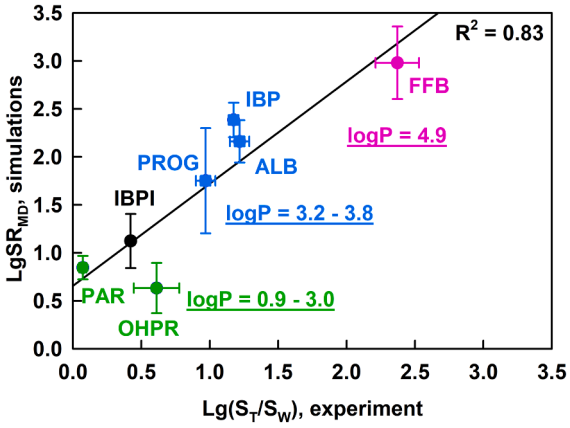

Fig. 3. Correlation plot between experimentally estimated and MD simulated solubility enhancement for the drug molecules into a mixed micelle of TC and DOPC. Neutral ibuprofen is denoted as IBP, whereas the ionized drug is marked as IBPI (black circle).

and charged drugs. However, additional factors such as negatively vs. positively charged drugs and charge location should be studied to explore whether the proposed approach can comprehensively replicate all effects of electrostatic interactions on solubilization.

To further analyze the validity of the obtained results, a comparison with literature data about micelle size and solubilization in similar systems was performed (Table 3). The micelle sizes of the intestinal micelles obtained in this study are in very good agreement with previously reported values [21]. CG simulations have also shown good agreement with the experimentally measured micelle size and have qualitatively replicated drug solubilization [16,22]. The advantage of the atomistic-level simulations used in the current study is in their ability to assess explicitly the role of hydrogen bonding and the interactions between all parts and atoms of the molecules in the micelles, which are essential for understanding solubilization. In addition, the proposed approach was optimized in respect to the required computational resources by working with a single micelle in a relatively small box. The main caveat in this case is that micelle – micelle interactions cannot be studied, unless the box size is increased, and more micelles are added (which would significantly increase computational costs). Drug – drug interactions could be easily assessed by including more than 1 drug molecule in the simulation and the effect of the size of the micelle on solubilization could be studied by varying the initial box size and number of molecules.

D. Drug-micelle and drug-water interactions

Hydrophobic interactions are expected to be among the main driving forces for solubilization of hydrophobic molecules into the hydrophobic environment of the micelles. In the current study, they were assessed by the RDF between micelle and drug in terms of solubilization – the highest SE was obtained for the most hydrophobic drug (fenofibrate) with the highest Log*P* due to the strong hydrophobic interactions between the drug molecule and the residues forming the hydrophobic micelle core. An additional indication for that is the number of contacts between drug and micelle, which was the highest for fenofibrate (Fig. S5 in the SI).

In addition to the hydrophobic interactions, there are possibilities for hydrogen bond formation between the drug and micelle. These polar interactions of the drug with the micelle and water were characterized by analyzing the most probable number of hydrogen bonds (Fig. 4). The most probable numbers are calculated as the percentage of the given number from the distribution plots of the number of hydrogen bonds in the last 100 ns of the simulations (Fig. S11 in the SI).

All drugs formed hydrogen bonds with taurocholate and water but not with DOPC. Except for FFB, all studied drug molecules formed at least one hydrogen bond with water and always more compared to TC. Practically, FFB did not form robust hydrogen bonds neither with TC,

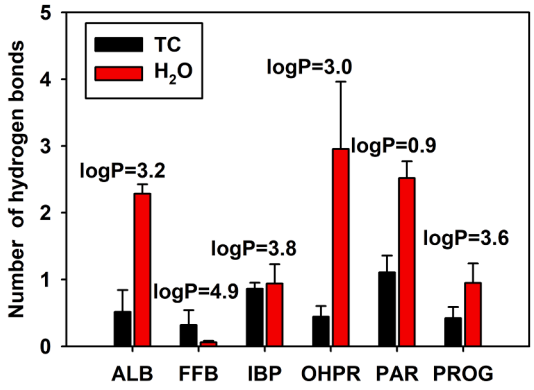

Fig. 4. Number of hydrogen bonds between drug molecules and TC (black bars) and water (red bars). (For interpretation of the references to colour in this figure legend, the reader is referred to the web version of this article.)

Table 3
Summary of computational approaches for estimating micelle size and solubilization.

Source	System composition	Box size, nm	Method	R_g (micelle), nm	Solubilization estimation	Comparison of solubilization with experiment
Current paper	40 TC 10 DOPC1 drug (6 different)	8	AA-MD	1.97–2.15	Solubilization enhancement calculated by RDF	quantitative
[16]	26–45 BS 4–16 PL 12–33 FA 1–2 drugs (3 different)	45	CG-MD	1.00–3.50	Micellar affinity calculated by number of contacts	qualitative
[19]	11–25 TC 5–3 DLiPC 1 drug	8.5	CG-MD	1.40–1.58	Free energy profiles	no
	160 TC 40 DLiPC 1 drug	12.1–12.9	CG-MD	2.94–3.06		
[21]	15–80 CH 60 DPC (no drug)	5.6	AA-MD	1.71–1.82	Solubilization was not studied	
[22]	24–193 CH 6–48 POPC (no drug)	20–30	CG-MD	1.3–1.90	Solubilization was not studied	

TC – taurocholate; PL – phospholipid; FA – fatty acid; CH – cholate; AA-MD – all-atom molecular dynamics; CG-MD – coarse grain molecular dynamics.

nor with water. This behavior is related to the position of the drug in the micelle: FFB was solubilized into the hydrophobic core of the micelles, where its access to the H-bond acceptors and donors of the other molecules was limited.

Overall, all drugs formed maximum one robust hydrogen bond with TC. Mostly, they formed hydrogen bonds with water and their number depended on the number of H-bond acceptors and mainly donors in the drug molecules (Table S4 in the SI) and their position in the micelle. Progesterone and ibuprofen formed one hydrogen bond with water, having 0 and 1 donors, and 2 acceptors, respectively. In contrast, albendazole (2 donors and 3 acceptors), OH-progesterone (1 donor and 3 acceptors) and paracetamol (2 donors and 2 acceptors) formed at least 3 HB or more with water. However, ionized IBP formed 5 HB with water, which is 5-fold more than the protonated molecules, due to the charge-dipole interactions with water and charge-charge interactions with surrounding sodium cations, reducing the solubilization (Fig. S10 in the SI).

The above results clearly illustrate the impact of molecular structure on location, orientation and solubilization of drug molecules. The most striking and easiest to interpret example is that of PROG vs. OHPR. Addition of a single OH-group to the molecule of PROG results in significant decrease of solubilization (Table 2), which is linked to the relocation of the molecule from the hydrophobic core to the palisade layer (Fig. 2). The analysis of the interactions presented in the current section shows that the driving force for this qualitatively different behavior of OHPR is the formation of much more hydrogen bonds with the water molecules, compared to PROG.

Finally, the energetics of drug solubilization were assessed by the molecular mechanics-Poisson-Boltzmann surface area method and a relatively good correlation between the total free energy and solubilization was observed for several of the studied molecules (Fig. S12 in the SI).

To summarize, three groups of drugs could be identified: (1) highly hydrophobic molecules solubilized into the micelle core (fenofibrate, Log$P \geq 4.9$), for which the main stabilizing forces were hydrophobic interactions with the oleic acid chains of the phospholipid, as previously shown for POPC [20,22] and oleic acid [49], (2) molecules with intermediate hydrophobicity, solubilized at least partially in the palisade layer (progesterone, neutral ibuprofen, albendazole, Log$P$ = 3.2–3.8), for which the location and orientation within the micelles was determined by the interplay between hydrogen bonds and hydrophobic forces and (3) molecules with low hydrophobicity (Log$P < 3.2$) and improved ability to form many (>3) hydrogen bonds, which were solubilized in the palisade layer near the surface of the micelle (ionized ibuprofen, hydroxyprogesterone, paracetamol).

4. Conclusions

We investigated the solubilization of hydrophobic molecules in a mixed intestinal micelle composed of taurocholate and phospholipid (DOPC) [50] by all-atom molecular dynamics simulations in explicit aqueous environment. To enable quantitative comparison of simulation results with experimental data, which was not previously achieved [24,25], we studied six drug molecules and obtained good correlation (R^2 = 0.83) between a simulation-derived parameter and the experimentally measured drug solubilization. In addition, the position and orientation of the solubilized drug in the micelle was determined by using cumulative number RDF and the geometrical center of the micelle as a reference initial point, instead of distributive RDF and center of atomic masses of the micelle [20]. This methodology avoids cumbersome calculations of partition coefficients and has a more general applicability than other approaches. Based on the above data, we were able to establish for the first time a quantitative correlation between Log$P$ and the position of the drug solubilized in an intestinal micelle, and to clarify the main interactions and forces governing solubilization. It could be used for CG simulations of the systems with a larger number of micelles and drug molecules without any modifications.

The results of the study advance the understanding and modelling of solubilization by: (1) Highlighting the key role of hydrogen bonding for the location, orientation and solubilization of drug molecules in intestinal micelles, (2) Providing methodological guidelines for future computational studies of solubilization, extending the currently available knowledge in this area [18,19,51,52] (several recent studies use coarse-grained models, in which hydrogen bonding was not discussed or was not taken into account explicitly [15,16,23,24]) and (3) Demonstrating good quantitative correlation ($R^2 = 0.83$) between a simulation-derived parameter and the experimentally measured drug solubilization ratio and Log$P$ for six drug molecules, in contrast to qualitative comparisons in the literature [24,25].

It is important to note, the main limitations of the method are that (1) it is not suitable to study slow processes (with characteristic times of the order of μs and above) and that (2) working at dilute conditions (e.g. few mmol/L) requires very big simulation boxes with millions/billions of water molecules, which require enormous computational resources. Both of these limitations can be considered as general limitations of the atomistic-level computational framework used in such MD studies.

Building on atomistic-level simulations like the present study, future efforts should focus on simulating larger biorelevant colloids (vesicles and nanodroplets) that may have an even more enhanced impact on drug solubilization *in vivo*. As such studies cannot be handled by atomistic-level simulations but by less detailed methods such as coarse-grained or dissipative particle dynamics, their development and verification with focus on the explicit implementation of hydrogen bonding will be crucial for advancing the understanding and computational studies of solubilization.

CRediT authorship contribution statement

Fatmegyul Mustan: Writing – review & editing, Writing – original draft, Resources, Methodology, Investigation, Formal analysis, Data curation. **Nikola Genchev:** Investigation. **Liliya Vinarova:** Methodology, Investigation. **Jan Bevernage:** Writing – review & editing, Validation, Conceptualization. **Christophe Tistaert:** Writing – review & editing, Validation, Conceptualization. **Anela Ivanova:** Writing – review & editing, Supervision, Resources, Methodology, Data curation. **Slavka Tcholakova:** Writing – review & editing, Conceptualization. **Zahari Vinarov:** Writing – review & editing, Validation, Project administration, Funding acquisition, Conceptualization.

Declaration of competing interest

The authors declare that they have no known competing financial interests or personal relationships that could have appeared to influence the work reported in this paper.

Acknowledgements

The authors are grateful to the Operational Program “Science and Education for Smart Growth” under contract UNITe No BG05M2OP001-1.001-0004-C01 (2018–2023) for the allocated computational time, to Johnson & Johnson Innovative Medicine for the support and to European Union-Next Generation EU, through the National Recovery and Resilience Plan of the Republic of Bulgaria, project No BG-RRP-2.004-0008. ZV and FM thank the National Research Program “VIHREN-2021”, project 3D-GUT (No KP-06-DV- 3/15.12.2021) for the support. Teodor Boyanov and Yoana Petrova are acknowledged for measuring some of the experimental solubilization data.

Appendix A. Supplementary data

Supplementary data to this article can be found online at https://doi.org/10.1016/j.jcis.2025.01.088.

Data availability

Data will be made available on request.

References

[1] G. Amidon, W. Higuchi, N. Ho, Theoretical and experimental studies of transport of micelle-solubilized solutes, J. Pharm. Sci. 71 (1) (1982) 77–84, https://doi.org/10.1002/jps.2600710120.

[2] A.J. Dahan, J.M. Miller, The solubility–permeability interplay and its implications in formulation design and development for poorly soluble drugs, AAPS J. 14 (2012) 244–251, https://doi.org/10.1208/s12248-012-9337-6.

[3] A. Dahan, A. Beig, D. Lindley, J.M. Miller, The solubility–permeability interplay and oral drug formulation design: two heads are better than one, Adv. Drug Deliv. Rev. 101 (2016) 99–107, https://doi.org/10.1016/j.addr.2016.04.018.

[4] J.M. Miller, A. Beig, B.J. Krieg, R.A. Carr, T.B. Borchardt, et al., The solubility–permeability interplay: mechanistic modeling and predictive application of the impact of micellar solubilization on intestinal permeation, Mol. Pharmaceut. 8 (5) (2011) 1848–1856, https://doi.org/10.1021/mp200181v.

[5] C. Fink, D. Sun, K. Wagner, M. Schneider, H. Bauer, et al., Evaluating the role of solubility in oral absorption of poorly water-soluble drugs using physiologically-based pharmacokinetic modeling, Clin. Pharmacol. Ther. 107 (3) (2020) 650–661, 10.1002%2Fcpt.1672.

[6] D. Dahlgren, H. Lennernäs, Intestinal permeability and drug absorption: predictive experimental, computational and in vivo approaches, Pharmaceutics 11 (2019) 411, https://doi.org/10.3390/pharmaceutics11080411.

[7] R. Holm, A. Mullertz, H. Mu, Bile salts and their importance for drug absorption, Int. J. Pharm. 453 (2013) 44–55, https://doi.org/10.1016/j.ijpharm.2013.04.003.

[8] P. Augustijns, B. Wuyts, B. Hens, P. Annaert, J. Butler, et al., A review of drug solubility in human intestinal fluids: Implications for the prediction of oral absorption, Euro. J. Pharm. Sci. 57 (2014) 322–332, https://doi.org/10.1016/j.ejps.2013.08.027.

[9] E. Enright, S. Joyce, C. Gahan, B. Griffin, The impact of gut microbiota-mediated bile acid metabolism on the solubilization capacity of bile salt micelles and drug solubility, Mol. Pharmaceut. 14 (4) (2017) 1251–1263, https://doi.org/10.1021/acs.molpharmaceut.6b01155.

[10] Z. Vinarov, M. Abdallah, J.A.G. Agundez, K. Allegaert, A.W. Basit, et al., Impact of gastrointestinal tract variability on oral drug absorption and pharmacokinetics: an UNGAP review, Eur. J. Pharm. Sci. 162 (2021) 105812, https://doi.org/10.1016/j.ejps.2021.105812.

[11] M. Koziolek, S. Alcaro, P. Augustijns, A.W. Basit, M. Grimm, et al., The mechanisms of pharmacokinetic food-drug interactions – a perspective from the UNGAP group, Eur. J. Pharm. Sci. 134 (2019) 31–59, https://doi.org/10.1016/j.ejps.2019.04.003.

[12] S. Pathak, A. Ruff, E. Kostewicz, N. Patel, D. Turner, et al., Model-based analysis of biopharmaceutic experiments to improve mechanistic oral absorption modeling: an integrated in vitro in vivo extrapolation perspective using ketoconazole as a model drug, Mol. Pharmaceut. 14 (2017) 4305–4320, https://doi.org/10.1021/acs.molpharmaceut.7b00406.

[13] N. Parrott, V. Lukacova, G. Fraczkiewicz, M.B. Bolger, Predicting pharmacokinetics of drugs using physiologically based modeling—application to food effects, AAPS J. 11 (1) (2009) 45–53, https://doi.org/10.1208/s12248-008-9079-7.

[14] T. Belubbi, D. Bassani, D. Stillhart, N. Parrott, Physiologically based biopharmaceutics modeling of food effect for basmisanil: a retrospective case study of the utility for formulation bridging, Pharmaceutics 15 (2023) 191, https://doi.org/10.3390/pharmaceutics15010191.

[15] A. Kabedev, S. Hossain, M. Hubert, P. Larsson, C.A.S. Bergstrom, Molecular dynamics simulations reveal membrane interactions for poorly water-soluble drugs: impact of bile solubilization and drug aggregation, J. Pharm. Sci. 110 (2021) 176–185, https://doi.org/10.1016/j.xphs.2020.10.061.

[16] A. Parrow, P. Larsson, P. Augustijns, C.A.S. Bergstrom, Molecular dynamics simulations of self-assembling colloids in fed-state human intestinal fluids and their solubilization of lipophilic drugs, Mol. Pharmaceut. 20 (2023) 451–460, https://doi.org/10.1021/acs.molpharmaceut.2c00710.

[17] T. Adelusi, A.-Q. Oyedele, I. Boyenle, A. Ogunlana, R. Adeyemi, et al., Molecular modeling in drug discovery, Inf. Med. Unlocked 29 (2022) 100880, https://doi.org/10.1016/j.imu.2022.100880.

[18] A.G. Guruge, D.B. Warren, C.W. Pouton, D.K. Chalmers, Molecular dynamics simulation studies of bile, bile salts, lipid-based drug formulations, and mRNA–lipid nanoparticles: a review, Mol. Pharmaceut. 20 (2023) 2781–2800, https://doi.org/10.1021/acs.molpharmaceut.3c00049.

[19] A. Kabedev, S. Hossain, Molecular dynamics simulations as a tool to understand drug solubilization in pharmaceutical systems, Comprehens. Comput. Chem. 3 (2024) 865–885, https://doi.org/10.1016/B978-0-12-821978-2.00114-8.

[20] S.J. Marrink, A.E. Mark, Molecular dynamics simulations of mixed micelles modeling human bile, Biochemistry 41 (17) (2002) 5375–5382, https://doi.org/10.1021/bi015613i.

[21] A. Sayyed-Ahmad, L. Lichtenberger, A. Gorfe, Structure and dynamics of cholic acid and dodecylphosphocholine–cholic acid aggregates, Langmuir 26 (16) (2010) 13407–13414, https://doi.org/10.1021/la102106t.

[22] E. Tuncer, B. Bayramoglu, Characterization of the self-assembly and size dependent structural properties of dietary mixed micelles by molecular dynamics simulations, Biophys. Chem. 248 (2019) 16–27, https://doi.org/10.1016/j.bpc.2019.02.001.

[23] A. Clulow, A. Parrow, A.M. Hawley, J. Khan, A. Pham, et al., Characterization of solubilizing nanoaggregates present in different versions of simulated intestinal fluid, J. Phys. Chem. B 121 (48) (2017) 10869–10881, https://doi.org/10.1021/acs.jpcb.7b08622.

[24] W.A. Birru, D.B. Warren, S. Han, H. Benameur, C.H.J. Porter, et al., Computational and experimental models of the gastrointestinal environment 2. Phase behavior and drug solubilization capacity of a Type I lipid-based drug formulation after digestion, Mol. Pharmaceut. 14 (3) (2017) 580–592, https://doi.org/10.1021/acs.molpharmaceut.6b00887.

[25] A. Parrow, P. Larsson, P. Augustijns, C.A.S. Bergström, Molecular dynamics simulations on interindividual variability of intestinal fluids: impact on drug solubilization, Mol. Pharmaceut. 17 (2020) 3837–3844, https://doi.org/10.1021/acs.molpharmaceut.0c00588.

[26] W.D. Cornell, P. Cieplak, C.I. Bayly, I.R. Gould, Merz, et al., A second generation force field for the simulation of proteins, nucleic acids, and organic molecules, J. Am. Chem. Soc. 117 (1995) 5179–5197, https://doi.org/10.1021/ja00124a002.

[27] I.R. Gould, A.A. Skjevik, C.J. Dickson, B.D. Madej, R.C. Walker, Lipid17: a comprehensive AMBER force field for the simulation of zwitterionic and anionic lipids, 2018, manuscript in preparation.

[28] W.L. Jorgensen, J. Chandrasekhar, J.D. Madura, R.W. Impey, M.L. Klein, Comparison of simple potential functions for simulating liquid water, J. Chem. Phys. 79 (1983) 926–935, https://doi.org/10.1063/1.445869.

[29] F. Mustan, A. Ivanova, G. Madjarova, S. Tcholakova, N. Denkov, Molecular dynamics simulation of the aggregation patterns in aqueous solutions of bile salts at physiological conditions, J. Phys. Chem. B 119 (2015) 15631–15643, https://doi.org/10.1021/acs.jpcb.5b07063.

[30] J. Wang, R.M. Wolf, J.W. Caldwell, P.A. Kollman, D.A. Case, Development and testing of a general amber force field, J. Comput. Chem. 25 (2003) 9, https://doi.org/10.1002/jcc.20035.

[31] A.D. Becke, Density-functional exchange-energy approximation with correct asymptotic behavior, Phys. Rev. a: at., Mol., Opt. Phys. 38 (1988) 3098–3100, https://doi.org/10.1103/PhysRevA.38.3098.

[32] A.D. Becke, Density-functional thermochemistry. III. The role of exact exchange, J. Chem. Phys. 98 (1993) 5648–5652, https://doi.org/10.1063/1.464913.

[33] R. Ditchfield, W.J. Hehre, J.A. Pople, Self-consistent molecular-orbital methods. IX. An extended Gaussian-type basis for molecular-orbital studies of organic molecules, J. Chem. Phys. 54 (1971) 724–728, https://doi.org/10.1063/1.1674902.

[34] C.I. Bayly, P. Cieplak, W.D. Cornell, P.A. Kollman, A well behaved electrostatic potential based method using charge restraints for deriving atomic charges – the RESP, Model. J. Phys. Chem. 97 (1993) 10269–10280, https://doi.org/10.1021/j100142a004.

[35] P. Cieplak, W.D. Cornell, C. Bayly, P.A. Kollman, Application of the multimolecule and multiconformational RESP methodology to biopolymers – charge derivation for DNA, RNA, and proteins, J. Comput. Chem. 16 (1995) 1357–1377, https://doi.org/10.1002/jcc.540161106.

[36] C. Zhu, R.H. Byrd, J. Nocedal, L-BFGS-B: algorithm 778: L-BFGS-B, FORTRAN routines for large scale bound constrained optimization, ACM Trans. Math. Softw. 23 (1997) 550–560, https://doi.org/10.1145/279232.279236.

[37] H.J.C. Berendsen, J.P.M. Postma, W.F. van Gunsteren, A. DiNola, J.R. Haak, Molecular-dynamics with coupling to an external bath, J. Chem. Phys. 81 (8) (1984) 3684–3690, https://doi.org/10.1063/1.448118.

[38] R.W. Hockney, S.P. Goel, J. Eastwood, Quiet high resolution computer models of a plasma, J. Comp. Phys. 14 (1974) 148–158, https://doi.org/10.1016/0021-9991(74)90010-2.

[39] J.-P. Ryckaert, G. Ciccotti, H.J.C. Berendsen, Numerical integration of the cartesian equations of motion of a system with constraints: molecular dynamics of n-alkanes, J. Comput. Phys. 23 (1977) 327–341, https://doi.org/10.1016/0021-9991(77)90098-5.

[40] S. Miyamoto, P.A. Kollman, Settle: an analytical version of the SHAKE and RATTLE algorithm for rigid water models, J. Comput. Chem. 13 (1992) 952–962, https://doi.org/10.1002/jcc.540130805.

[41] T. Darden, D. York, L. Pedersen, Particle mesh Ewald: an N·log(N) method for ewald sums in large systems, J. Chem. Phys. 98 (1993) 10089–10092, https://doi.org/10.1063/1.464397.

[42] U. Essmann, L. Perera, M.L. Berkowitz, T. Darden, H. Lee, L.G. Pedersen, A smooth particle mesh ewald method, J. Chem. Phys. 103 (1995) 8577–8593, https://doi.org/10.1063/1.470117.

[43] Lindahl, Abraham, Hess, and van der Spoel. GROMACS 2021.3 Manual (2021.3). Zenodo 2021 https://doi.org/10.5281/zenodo.5053220.

[44] W. Humphrey, A. Dalke, K.V.M.D. Schulten, Visual molecular dynamics, J. Mol. Graphics 14 (1996) 33–38, https://doi.org/10.1016/0263-7855(96)00018-5.

[45] A. van der Bondi, Waals volumes and radii, J. Phys. Chem. 68 (1964) 441–451, https://doi.org/10.1021/j100785a001.

[46] M.C. Carey, D.M. Small, The characteristics of mixed micellar solutions with particular reference to bile, Am. J. Med. 49 (5) (1970) 590–608, https://doi.org/10.1016/S0002-9343(70)80127-9.

[47] J. Ulmius, G. Lindblom, H. Wennerstroem, J.L. Fontell, B.A.K. Molecular organization in the liquid-crystalline phases of lecithin-sodium cholate-water systems studied by nuclear magnetic resonance, Biochemistry 21 (7) (1982) 1553–1560, https://doi.org/10.1021/bi00536a014.

[48] J.W. Nichols, J. Ozarowski, Sizing of lecithin-bile salt mixed micelles by size-exclusion high-performance liquid chromatography, Biochemistry 29 (19) (1990) 4600–4606, https://doi.org/10.1021/bi00471a014.

[49] E. Tuncer, B. Bayramoglu, Molecular dynamics simulations of duodenal self assembly in the presence of different fatty acids, Colloids Surf., A 644 (2022) 128866, https://doi.org/10.1016/j.colsurfa.2022.128866.

[50] D. Riethorst, P. Baatsen, C. Remijn, A. Mitra, J. Tack, et al., An in-depth view into human intestinal fluid colloids: intersubject variability in relation to composition, Mol. Pharmaceutics 13 (10) (2016) 3484–3493, https://doi.org/10.1021/acs.molpharmaceut.6b00496.

[51] C. Bergström, W. Charman, C. Porter, Computational prediction of formulation strategies for beyond-rule-of-5 compounds, Adv. Drug Delivery Rev. 101 (2016) 6–21, https://doi.org/10.1016/j.addr.2016.02.005.

[52] S.R. Euston, Molecular simulation of biosurfactants with relevance to food systems, Curr. Opin. Colloid Interface Sci. 28 (2017) 110–119, https://doi.org/10.1016/j.cocis.2017.04.002.